International Journal of
Environmental Science
(IJES)

Comparison between Radiological Consequences of Several Studies for the Radioactive Source of Fukushima Accident Using Air Dispersion Model at Different Stability Class

O.S. Ahmed

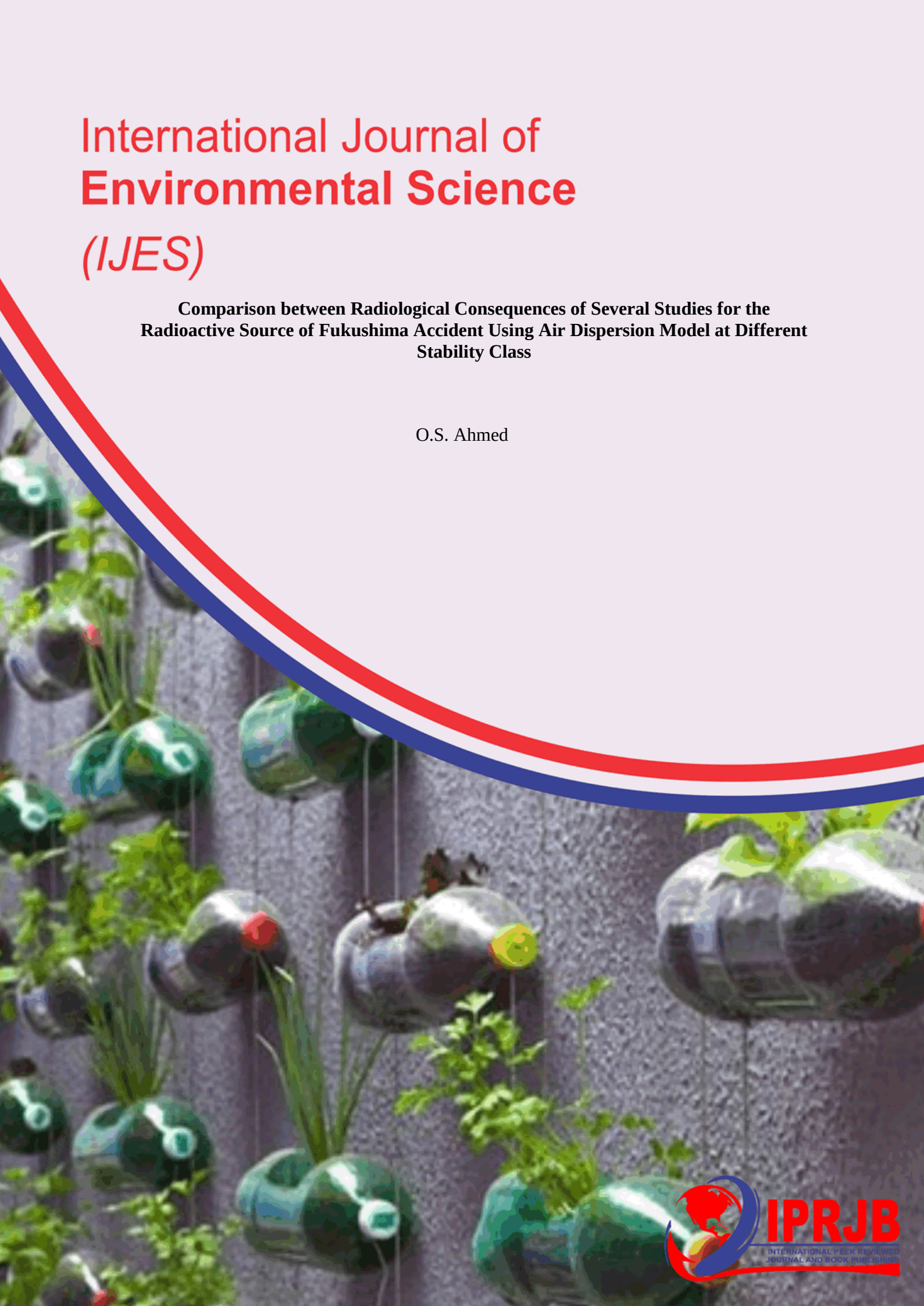

IPRJB
INTERNATIONAL PEER REVIEWED JOURNAL AND BOOK PUBLISHING

International Journal of Environmental Sciences
ISSN 2519-5549 (online)
Vol.9, Issue 1, No.1. pp 1 - 28, 2026

www.iprjb.org

Comparison between Radiological Consequences of Several Studies for the Radioactive Source of Fukushima Accident Using Air Dispersion Model at Different Stability Class

[1*]O.S. Ahmed
Department of Physics, College of Science, Qassim University, Saudi Arabia

Article History

Received 10th December 2025

Received in Revised Form 6th January 2026

Accepted 9th February 2026

How to cite in APA format:

Ahmed, O. (2026). Comparison between Radiological Consequences of Several Studies for the Radioactive Source of Fukushima Accident Using Air Dispersion Model at Different Stability Class. *International Journal of Environmental Sciences*, *9*(1), 1–28. https://doi.org/10.47604/ijes.3625

Abstract

The source term is important for computer simulations on the dispersion of radioactive materials in the environment. Several studies estimated the source term of cesium discharged to the atmosphere, the Total Effective Dose Equivalent (TEDE) resulting from release of Cs-137 at different stability class, in order to evaluate the radiological dose to the public resulting from the month-long discharge of radioactive materials into the atmosphere from the Fukushima Daiichi Nuclear Power Plant accident using Hotspot code. The contour map from program shows how radiological dose changes with direction and distance from the release point. Near the plume centerline, where atmospheric dispersion is least, the TEDE values are highest .Due to atmospheric dilution, radioactive decay, plume spreading (σ_y and σz increase), and the spatial distribution of Cs-137 ground deposition after plume passage, the dose decreases radially. Near the source and along the plume axis, ground deposition is at its maximum. Due to plume dilution and gravity settling, deposition diminishes with distance, and the long-lived radioactive Cs-137 poses a long-term contamination concern. Because TEDE rises quickly close to the source due to high plume concentration, TEDE changes with downwind distance from the source. The intersection of the breathing height and the plume centerline at an intermediate distance is where the maximum dose occurs. After vertical dispersion becomes effective, TEDE drops because of increased dilution. Plume arrival time strongly depends on stability class, which is important for emergency response and protective action planning, and necessary to consider atmospheric stability class characteristics in developing emergency preparedness and response strategies. The results showed that the largest inter-model differences occur near the source (< 1 km), while results converge at larger distances. Tabulated results show that RASCAL generally predicts the highest TEDE (most conservative), EAEA the lowest, and IRSN/Terada intermediate values. Maximum TEDE typically occurs at 0.4–0.6 km from the source.

Keywords: *Fukushima Daiichi Nuclear Power Plants, TEDE, Cs-137, HOTSPOT Code*

International Journal of Environmental Sciences
ISSN 2519-5549 (online)
Vol.9, Issue 1, No.1. pp 1 - 28, 2026

www.iprjb.org

INTRODUCTION

On March 11, 2011, a magnitude 9.0 earthquake off the coast of Japan and the ensuing tsunami caused the coolant systems of the Fukushima Daiichi Nuclear electricity Plants to lose electricity. When the earthquake struck, Units 1, 2, and 3 were in operation and automatically shut down. At the time of the earthquake, units 4, 5, and 6 were closed for maintenance and refueling [1-3]. Because the loss of coolant recirculation in units 1, 2, and 3 occur elevated temperatures and pressures in the containment vessels [4-8] . In order to lower the internal pressure, the containment containers of these units were released to the atmosphere after a few hours or days. Radioactive particles and gasses were released into the environment during the venting events. The values for Cs-137 that have been produced by multiple authors are displayed in Table (1). The public's radioactive exposure as a result of this leak must be evaluated immediately [1] [2] [3].The research simulated the radiation emission following the disaster using theoretical models. In this work, the radiation dose surrounding the nuclear site following the accident (within 100 km from the reactor) was simulated and assessed using a Gauss-plume model code (HOTSPOT). To ascertain the radiation dose and radioactive deposits in the soil surrounding the reactor, the HOTSPOT code was utilized with the source term computed by RASCAL 4.2, NSC, JNES, NISA, Terada as per IRSN, Terada (manual sum), Winiarek, Chino, NSC, and EAEA as input data.

Table 1: Cumulative Source Term (Bq) by Several Studies

T1/2 [d]	Nuclide	Reference	Value
1.10E+04	Cs-137	RASCAL 4.2 Total (ENEA)	2.14E+16
		NSC 22/08/2011 (8)	1.10E+16
		JNES (8)	6.10E+15
		NISA 16/2/2012 (9)	8.20E+15
		Terada as per IRSN (10)	1.3E+16
		Terada (manual sum) (11)	8.83E+15
		Winiarek (12)	1.20E+16
		Chino (13)	1.30E+16
		NSC (14)	1.20E+16
		Morino (15)	9.94E+15
		EAEA (16)	1.64E+15

MATERIALS AND METHODS

HotSpot is a free license code that offers a quick way to assess the radiation consequences of radioactive material releases into the atmosphere. It is based on a Gaussian model that calculates the short-term (less than a few hours) and short-range (less than 10 km) predictions for the radiological impact downwind after radioactive material is released [17]. The Gaussian model is used in HotSpot algorithms that deal with radioactive material dispersal because its suitability for initial dispersion estimations or worst-case safety calculations has been studied and confirmed for many years. The most recent and authorized radiological dosage conversion data and techniques are constantly incorporated into the codes. The well-known Gaussian Plume Model (GPM), which is frequently used for an initial emergency assessment or safety analysis planning of a radioactive release, is the foundation of this code. The Gaussian plume models' primary benefits are their quick computation times, thorough validation, and widespread global acceptance. The initial 3D distribution of material related to an explosive release, fire release, resuspension, or user-input geometry is modeled using virtual source terms. HotSpot employs

radiation dosimetry techniques suggested by the US Environmental Protection Agency [19] and the International Commission on Radiological Protection (ICRP) [18] for the assessment of radiological scenarios. The Pasquill classes can be chosen using HOT SPOT to replicate various weather conditions. The code employed the Gaussian numerical method of continuous release to ascertain the aerosol concentration in the atmosphere. All the information required to calculate dispersion is included in the Gaussian Eq. (1), which is explained as follows: flow rate, coefficient diffusion, effective release height, various atmospheric stabilities, wind speed and direction, and atmospheric conditions.

$$X(x,y,z,H) = \frac{Q}{2\pi u\sigma_y\sigma_z}\, e^{\frac{-y2}{2\sigma^2 y}}\left(e^{\frac{-(z-H)2}{2\sigma^2 z}} + e^{\frac{-(z+H)2}{2\sigma^2 z}}\right)e^{\frac{-\lambda x}{u}} \quad \ldots\ldots\ldots\ldots\ldots\ldots \quad (1)$$

If the height of mixing layer (h) is considered, and the vertical standard deviation exceeds the inversion height, Eq. (1) becomes:

$$X(x,y,z,H) = \frac{Q}{\sqrt{2\pi}uh\sigma_y}\exp\left[-\frac{y^2}{2\sigma_y^2}\right]\text{e^((- }\lambda\text{x)/u).....(2)}$$

Where :- X(x, y, z, H) represents the time integrated atmospheric concentration (Bq s m^{-3})

Q : a source term (Bq).

H is the effective stack height (m),

u is the average wind speed (m s^{-1}),

σy and σz are the horizontal and vertical standard deviations (m), respectively,

λ is the constant of radioactive decay (s^{-1}),

x is the distance downwind from the source (m),

y and z are the crosswind and vertical axis distances (m), respectively,

h describes the height (m) of the inversion layer.

METHODOLOGY

We chose to examine the dispersion of CS-137 in order to simulate the radionuclide dispersion during the event using scenario (General plume). Additionally, this work's primary goal was to assess its dispersion during the first hour of the accident based on the software's capabilities. the boundary conditions, the several states of the local atmosphere that meteorologists identify: A, B, C, D, E, and F the weather, wind speed, and time of day can all be used to calculate these states. The attack may have a variety of deadly consequences, depending on the stability class. Therefore, in order to maximize the deadly effects, the potential terrorist will undoubtedly take things into account, just as war planners do. The temperature differential between an air parcel and the surrounding air determines the stability of the atmosphere. As a result, the temperature differential between the air parcel and the surrounding air may determine varying degrees of stability [20]. Pasquill-Gifford stability is the name given to the stability classes utilized in this work [20]. Daytime hours with unstable conditions are referred to as stability classes A, B, and C. Neutral circumstances and cloudy days or nights are represented by stability D. Stabilities E and F are dependent on the degree of cloud cover and relate to stable circumstances during the night. As a result, the most unstable conditions are represented by classification A, and the

most stable conditions are represented by classification F. The simulation makes use of Select the "General Plume" model to replicate the best-case scenario for radioactive leakage from a chimney. Following that, the primary boundary conditions were added to the software's GUI (Graphical User Interface). In emergency situations, TED was evaluated using the HotSpot Health Physics Code [21-25]. Two deposition velocities 0.3 cm s^{-1} for respirable particles and non -respirable particles—were taken into consideration, and it was expected that the diffusion properties would stay constant throughout the release. The inversion layer height was set at 300 meters. According to the site's meteorological observations, the predominant wind direction was west-northwest (WNW), with a wind speed of 3 m s−1.The default value of receptor height was set at 1.5 m, and the TED computation was assessed at a distance of 5 km from the source. The emission point is ten meters high in both cases, and the sample duration is set at sixty minutes. The FGR 11 DFC library is utilized, which enables the inclusion of the phenomena of particle resuspension and reflection on the ground [20,21]. As stated for a population with medium intensity activity, the mean respiratory flow has been set at 3.33 x 10^{-4} m3/s. The levels of radioactivity on the ground have been added to the TEDE (Total Effective dose Equivalent) values, which are the sum of the equivalent dose for each organ in the body (both for internal and exterior deposition).

RESULTS AND DISCUSSION

The spatial distribution of Total Effective Dose Equivalent (TEDE) resulting from the atmospheric release of Cs-137 is shown in Figures 1a, 3a, 5a, 7a, 9a, 11a, 13a, 15a, and 17a. The total radiation dose that an individual receives from emitted Cs-137, including external exposure (cloud shine), is known as the Total Effective Dose Equivalent (TEDE). When the radioactive plume passed overhead, it released gamma radiation . Particles of Cs-137 that are ingested and deposited in the lungs due to internal exposure from the outside (ground shine) Cs-137 gamma radiation that was left on the earth. Figure (1a): RASCAL analysis: demonstrate Narrow, elongated plume with high TEDE close to the source Figure (3a): The NSC investigation demonstrates a broader lateral plume spread, a lower peak TEDE, and a peak dose reduction due to increased air dispersion,

Because of the changing weather and increased plume dilution caused by physical realism, the JNES study (Figure 5a) displays smooth TEDE gradients and dose distributes across a wider area. Due to simplified deposition physics, Figure (7a) of the NISA study shows a moderately high TEDE and a relatively narrow plume. Terada (IRSN) study, broad TEDE, several dose maxima (hotspots) because to particle dispersion, and explicit turbulent transport are shown in Figure (9a). Due to the aggregate of several release occurrences, the Terada (manual sum) study in Figure (11a) has a smoother spatial distribution and a higher cumulative TEDE. Figure (13a): The Winiarek study displays irregular TEDE patterns, a non-symmetric plume as a result of measurements-constrained inverse modeling, actual wind shifts, and turbulence. The Morino investigation (Figure 15a) demonstrates lower TEDE values, wide spatial dilution as a result of robust vertical mixing, effective aerosol removal, and dose reduction dominated by atmospheric cleansing. Due to long-range dispersion physics and regional-scale transport models, Figure (17a) of the EAEA study displays a very wide TEDE distribution, low peak dosage, and a huge affected area. general Wide plumes lead to an unstable atmosphere, narrow plumes lead to a stable atmosphere, and high TEDE hotspots lead to slow wind and poor mixing.

Figures (1b, 3b, 5b, 7b, 9b, 11b, 13b, 15b, and 17b) that highlight Cs-137 ground deposition contour plots The amount of radioactive Cs-137 extracted from the atmosphere and collected

on the surface is known as ground deposition (Bq/m2). Deposition happens through two primary mechanisms: Particle size, surface roughness, and wind speed all affect dry deposition caused by turbulent impaction on surfaces and gravity settling of particles. Rainfall intensity, cloud-plume interaction, precipitation timing in relation to plume passage, and washout and rain scavenging are all highly influenced by wet deposition (dominant for Cs-137). Figure (1b): Due to simplified Gaussian deposition, limited wet deposition treatment, and the assumption of constant deposition velocity, the RASCAL analysis reveals a narrow deposition plume, high deposition at the source, and quick reduction away.

Figure (3b) illustrates the NSC study's slightly broader plume, lower peak deposition as a result of better turbulence depiction, some atmospheric mixing prior to deposition, and more realistic Cs-137 elimination throughout transport . The JNES research in Figure (5b) displays smooth deposition contours, moderate hotspot intensity as a result of time-dependent meteorology, and partial wet deposition treatment. Over time, Cs-137 was gradually eliminated .Figure (7b): NISA analysis revealed a small geographical footprint and increased deposition around the plume centerline.

because the deposition coefficients are conservative . Strong localized hotspots, an uneven deposition pattern caused by explicit rainfall scavenging, and realistic turbulence are shown in Figure (9b) of the Terada (IRSN) investigation. Terada (manual sum) study (Figure 11b): observed overlapping plume trajectories, a wider deposition footprint, and a slightly lower peak intensity as a result of accumulation from several release episodes.The Winiarek study's highly irregular outlines and strong agreement with known hotspots are shown in Figure (13b), which includes real precipitation timing and inverse modeling constrained by measurements. Figure (15b): The Morino study demonstrates that broad but low-intensity deposition, good vertical mixing, and effective plume dilution prior to scavenging resulted in a decreased hotspot contrast. The EAEA research in Figure (17b) demonstrates a relatively wide deposition area, low peak values because of the regional-scale transport model, and long-range dispersion dominance.

International Journal of Environmental Sciences
ISSN 2519-5549 (online)
Vol.9, Issue 1, No.1. pp 1 - 28, 2026

www.iprjb.org

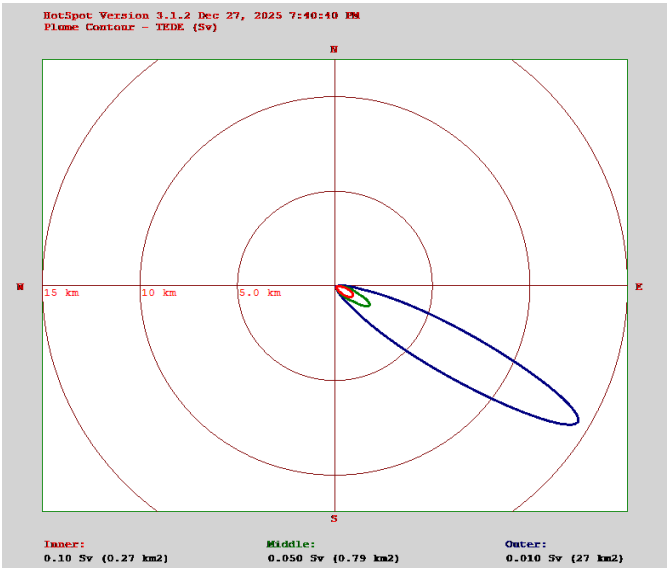

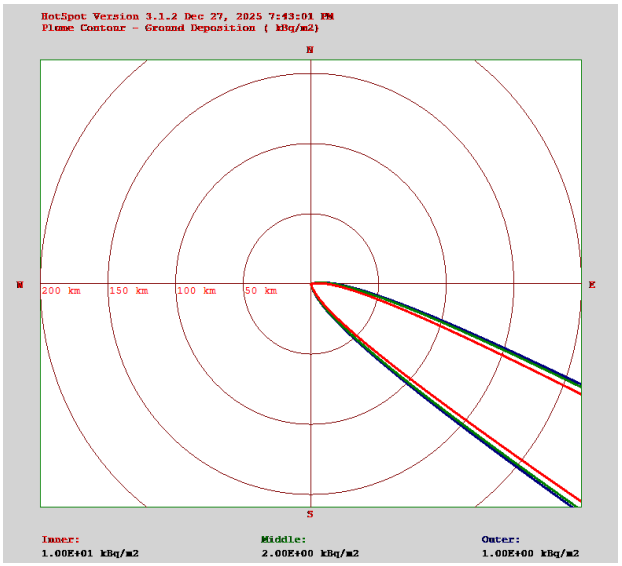

(a) (b)

Figure 1): Cs-137 in case RASCAL study (a) TEDE plot , (b) Ground deposition contour plot of

International Journal of Environmental Sciences
ISSN 2519-5549 (online)
Vol.9, Issue 1, No.1. pp 1 - 28, 2026

www.iprjb.org

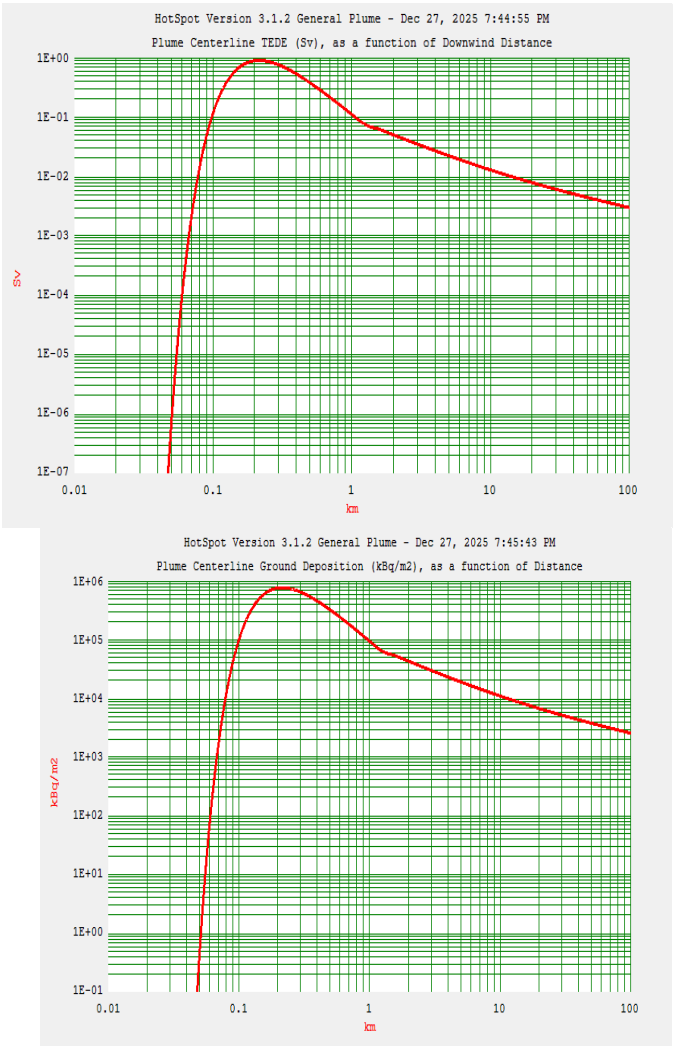

(a) (b)

Figure 2: Cs-137 in case RASCAL study (a) TEDE Graph , (b) Ground deposition Graph

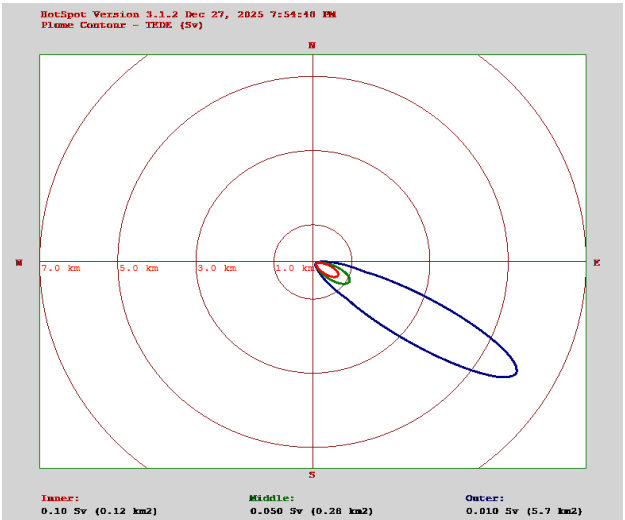

International Journal of Environmental Sciences
ISSN 2519-5549 (online)
Vol.9, Issue 1, No.1. pp 1 - 28, 2026

www.iprjb.org

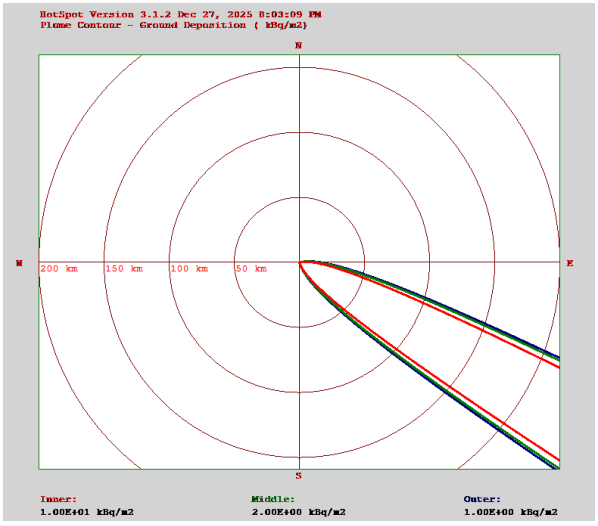

Figure 3: Cs-137 in case NSC study (a) TEDE plot , (b) Ground deposition contour plot of

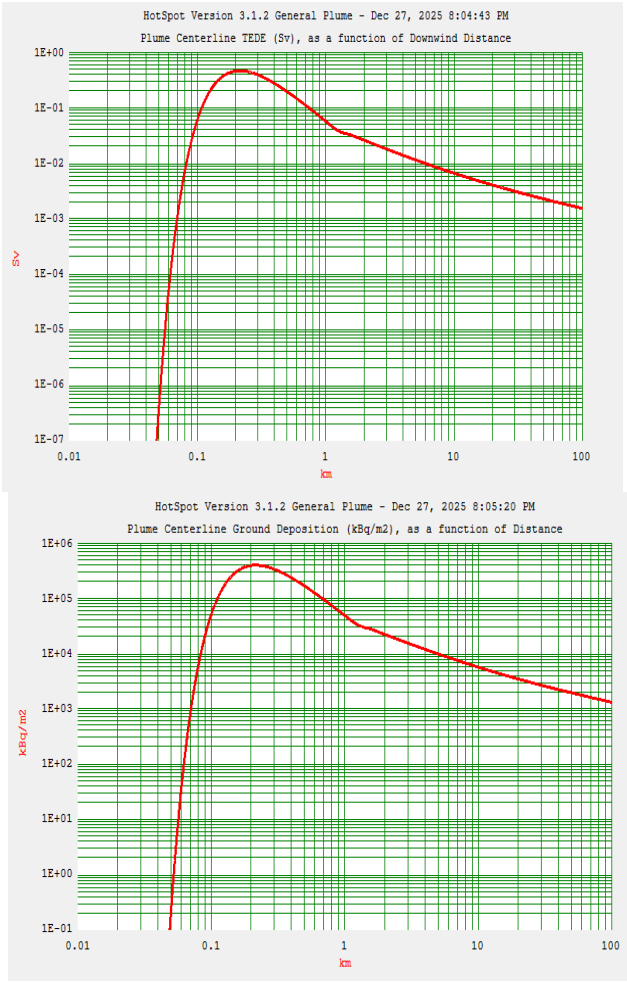

(a) (b)

Figure 4: Cs-137 in case NSC study (a) TEDE Graph , (b) Ground deposition Graph

International Journal of Environmental Sciences
ISSN 2519-5549 (online)
Vol.9, Issue 1, No.1. pp 1 - 28, 2026

www.iprjb.org

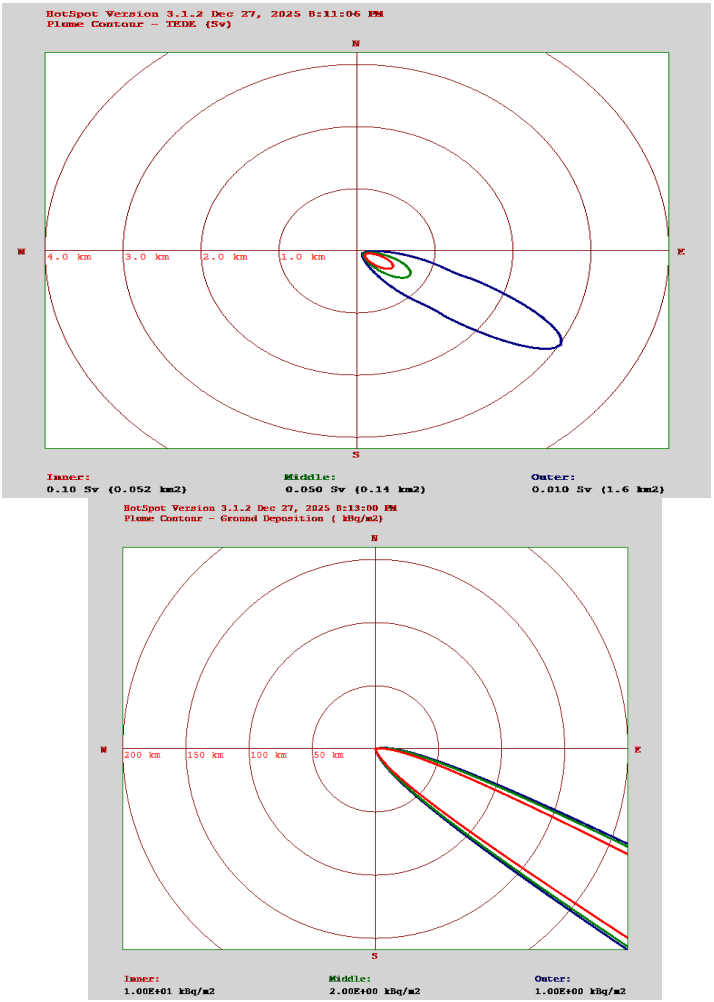

Figure 5: Cs-137 in case JNES study (a) TEDE plot , (b) Ground deposition contour plot of

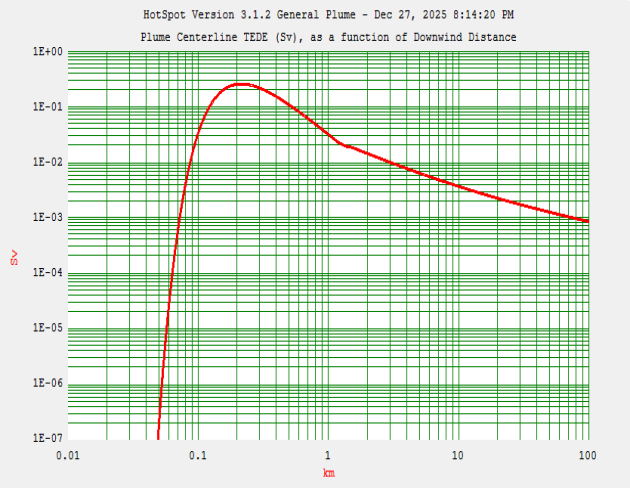

International Journal of Environmental Sciences
ISSN 2519-5549 (online)
Vol.9, Issue 1, No.1. pp 1 - 28, 2026

www.iprjb.org

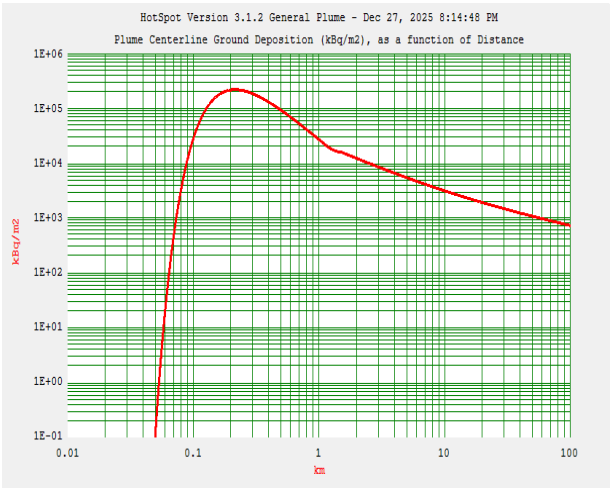

(a) (b)

Figure 6: Cs-137 in case JNES study (a) TEDE Graph , (b) Ground deposition Graph

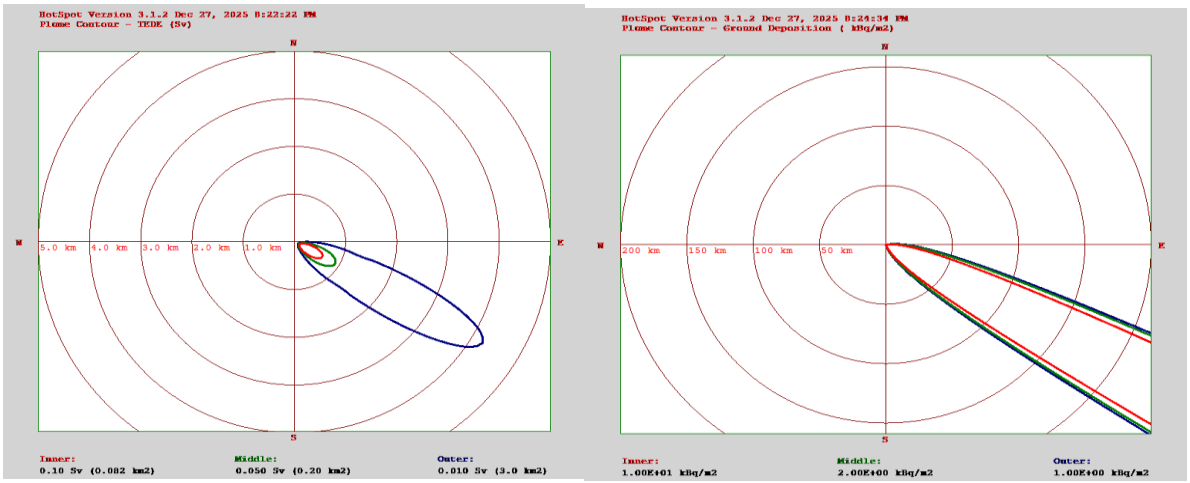

Figure 7:- Cs-137 in case NISA study (a) TEDE plot , (b) Ground deposition contour plot of

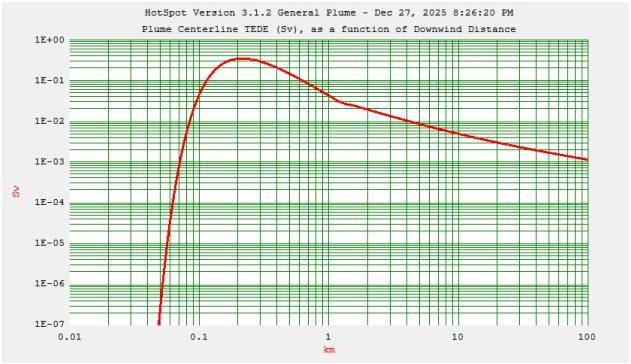

International Journal of Environmental Sciences
ISSN 2519-5549 (online)
Vol.9, Issue 1, No.1. pp 1 - 28, 2026

www.iprjb.org

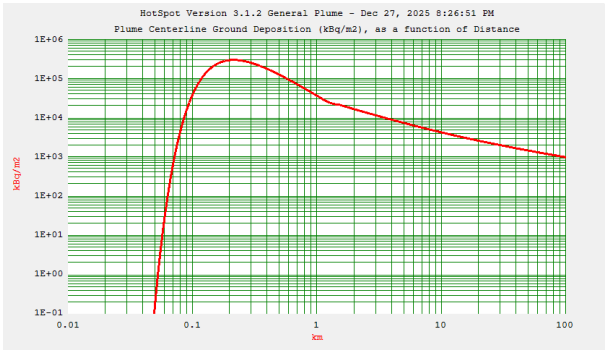

(a) (b)

Figure 8: Cs-137 in case NISA study (a) TEDE Graph , (b) Ground deposition Graph

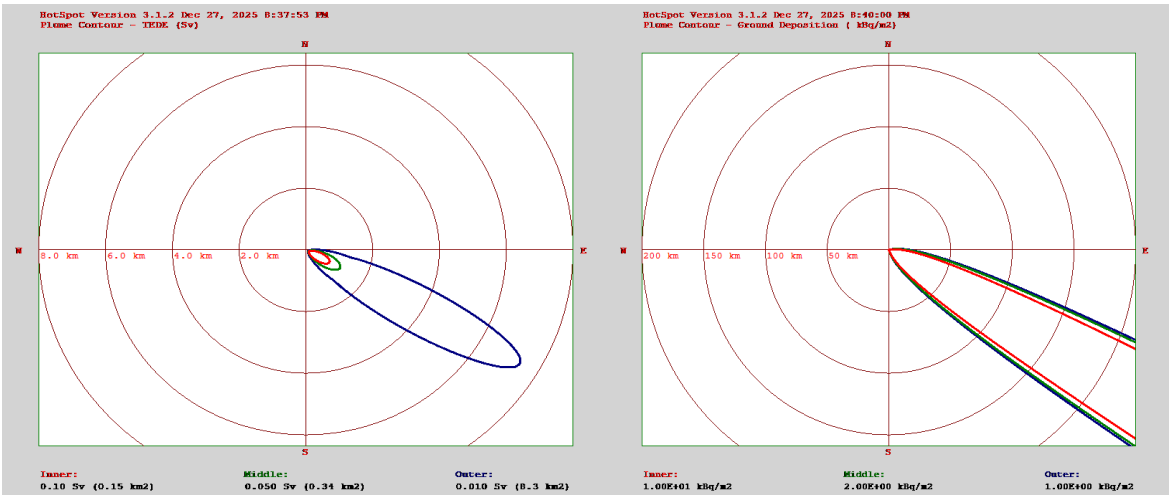

Figure(9):- Cs-137 in case Terada as per IRSN study (a) TEDE plot , (b) Ground deposition contour plot

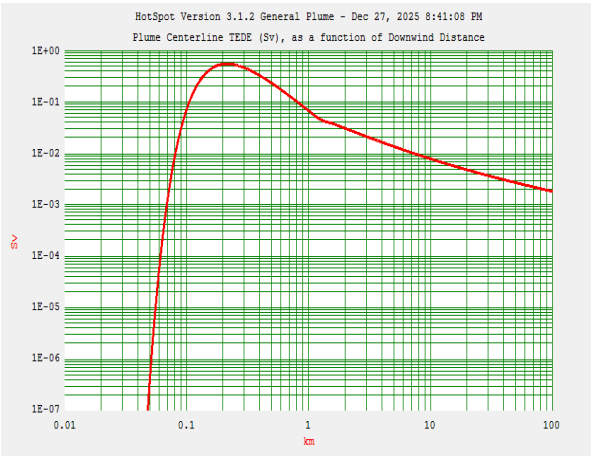

International Journal of Environmental Sciences
ISSN 2519-5549 (online)
Vol.9, Issue 1, No.1. pp 1 - 28, 2026

www.iprjb.org

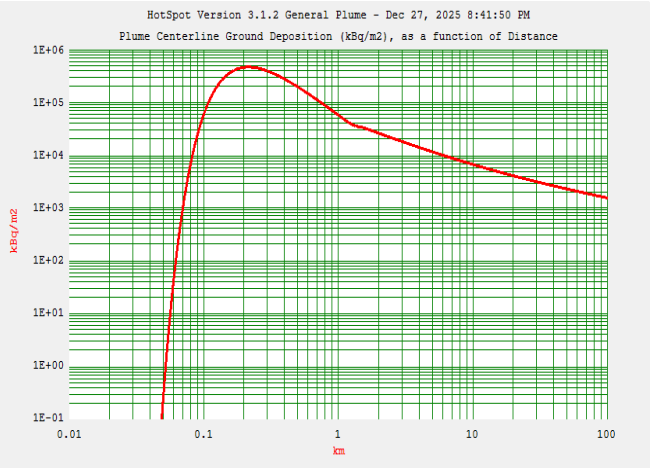

(a) (b)

Figure 10: Cs-137 in case Terada as per IRSN study (a) TEDE Graph , (b) Ground deposition Graph

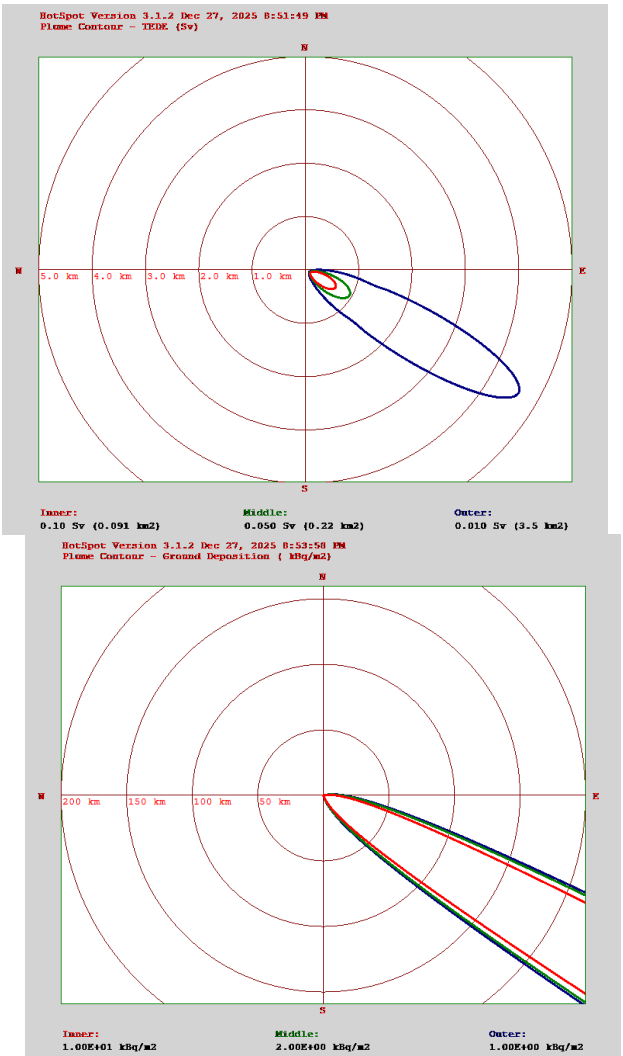

Figure 11: Cs-137 in case Terada (manual sum) study (a) TEDE plot , (b) Ground deposition contour

International Journal of Environmental Sciences
ISSN 2519-5549 (online)
Vol.9, Issue 1, No.1. pp 1 - 28, 2026
www.iprjb.org

plot

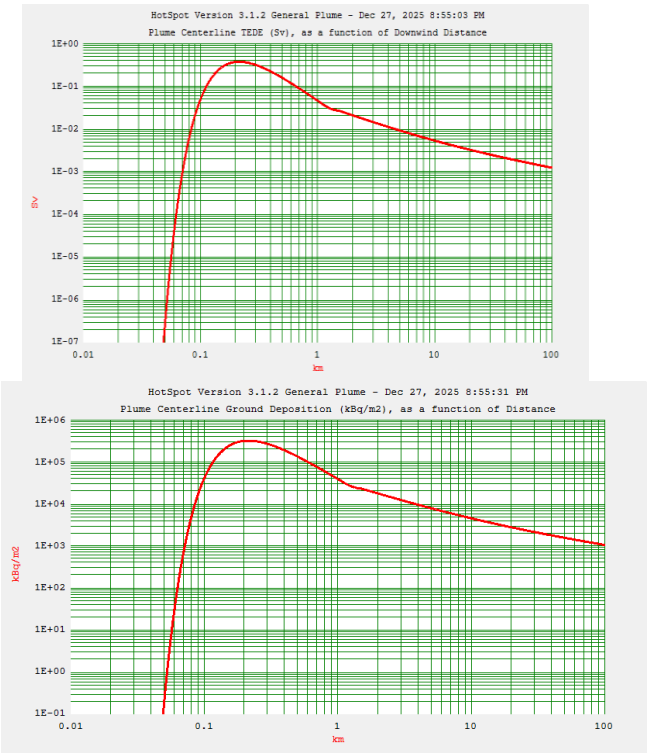

(a) (b)

Figure 12: Cs-137 in case Terada (manual sum) study (a) TEDE Graph , (b) Ground deposition Graph

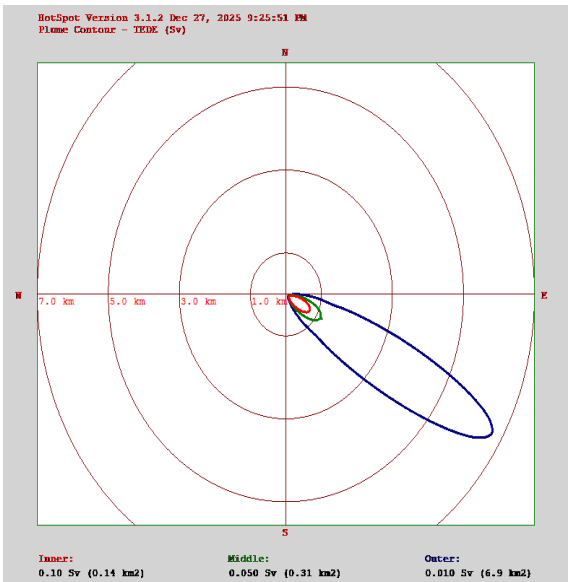

International Journal of Environmental Sciences
ISSN 2519-5549 (online)
Vol.9, Issue 1, No.1. pp 1 - 28, 2026

www.iprjb.org

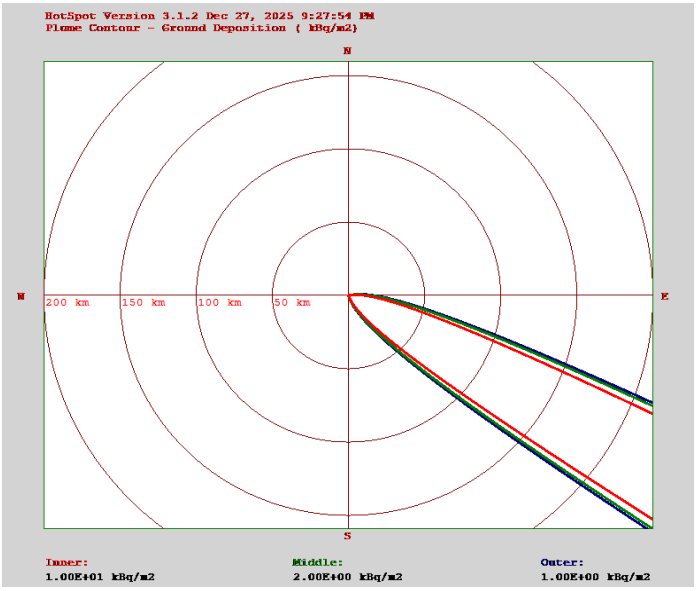

Figure 13: Cs-137 in case winiarek study (a) TEDE plot , (b) Ground deposition contour plot

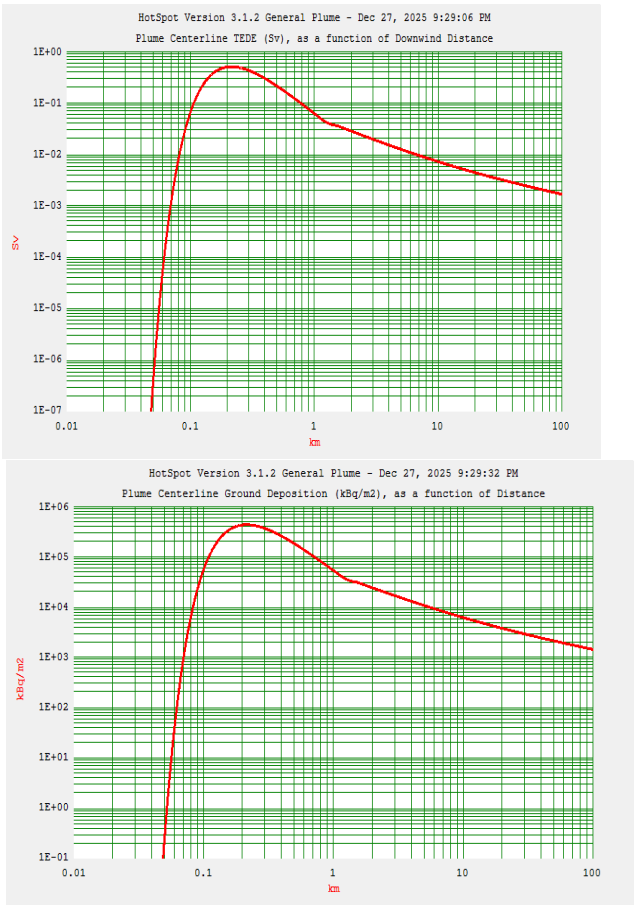

(a) (b)

Figure 14: Cs-137 in case winiarek study (a) TEDE Graph , (b) Ground deposition Graph

International Journal of Environmental Sciences
ISSN 2519-5549 (online)
Vol.9, Issue 1, No.1. pp 1 - 28, 2026

www.iprjb.org

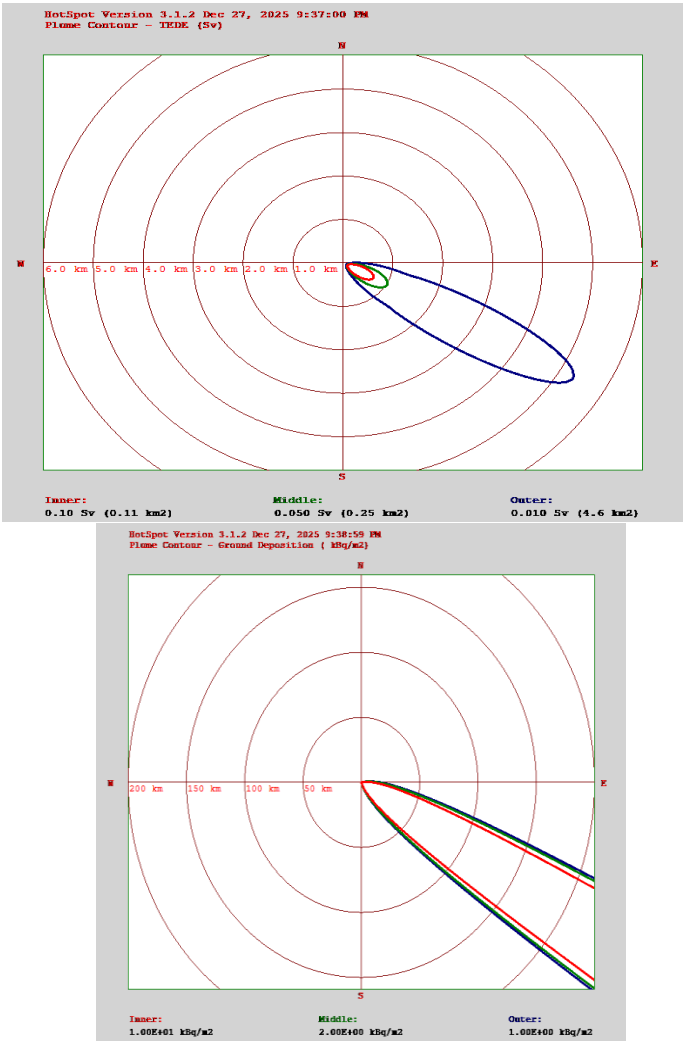

Figure 15:- Cs-137 in case morino study (a) TEDE plot , (b) Ground deposition contour plot

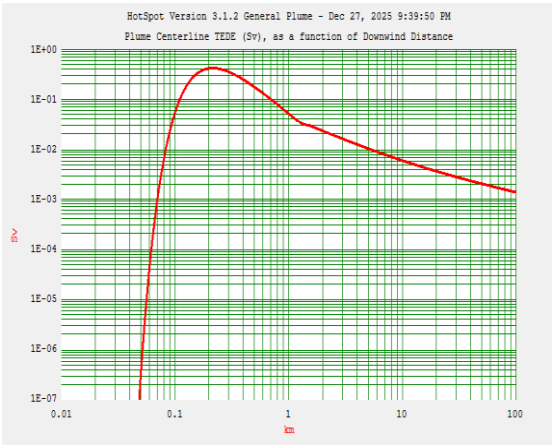

International Journal of Environmental Sciences
ISSN 2519-5549 (online)
Vol.9, Issue 1, No.1. pp 1 - 28, 2026

www.iprjb.org

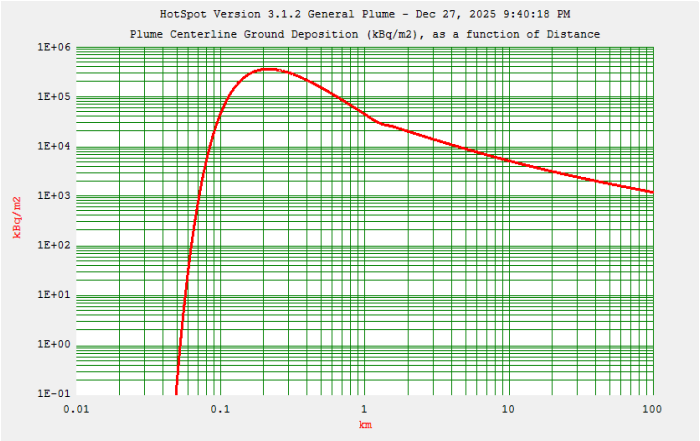

(a) (b)

Figure 16: Cs-137 in case morino study (a) TEDE Graph , (b) Ground deposition Graph

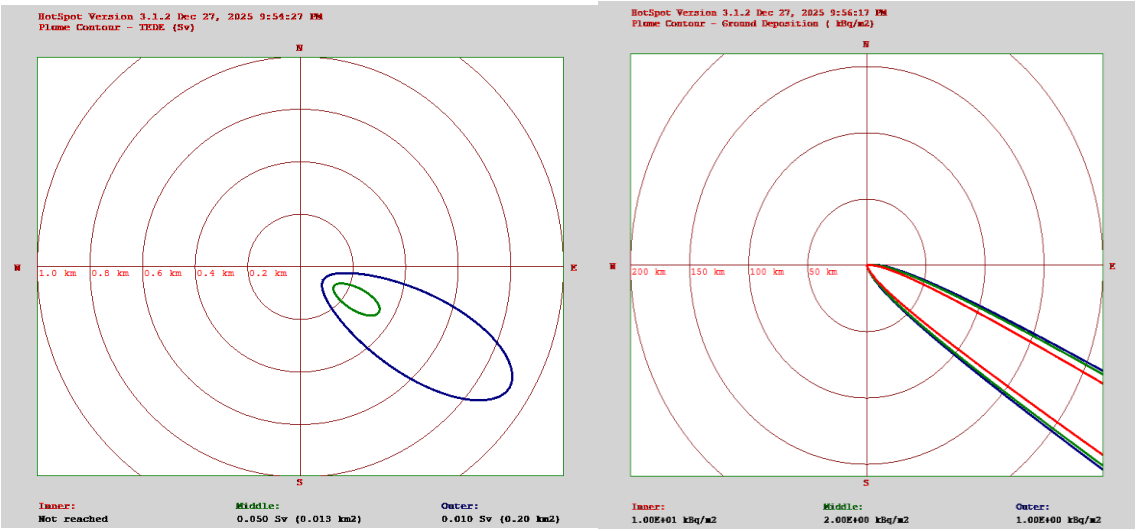

Figure 17: Cs-137 in case EAEAstudy (a) TEDE plot , (b) Ground deposition contour plot

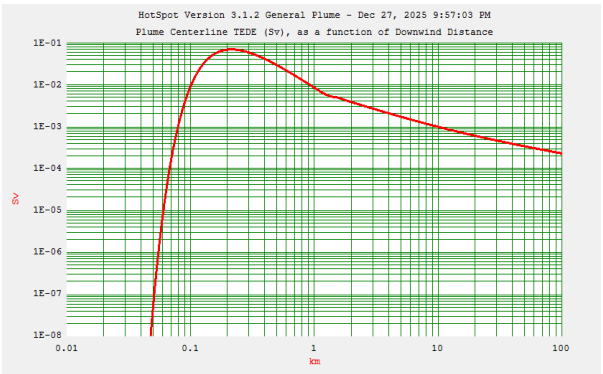

International Journal of Environmental Sciences
ISSN 2519-5549 (online)
Vol.9, Issue 1, No.1. pp 1 - 28, 2026
www.iprjb.org

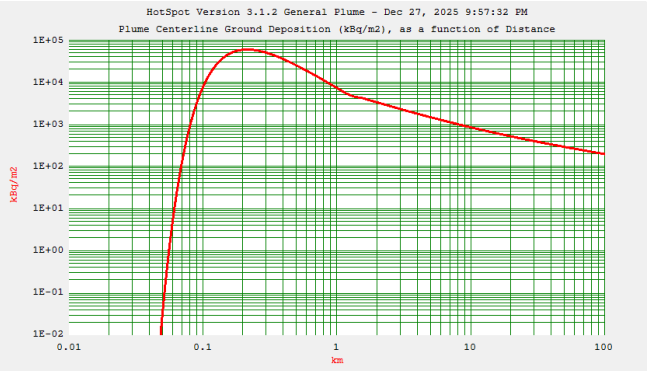

(a) (b)

Figure 18: Cs-137 in case EAEA study (a) TEDE Graph , (b) Ground deposition Graph

Figure (19) extremely erratic atmosphere (A), demonstrate Strong solar heating is followed by significant turbulence, quick vertical and horizontal plume spreading, and strong concentration dilution. The differences across models are greatest at short distances (<1 km) because of high TEDE close to the source . Simplified models (RASCAL, NSC) produce sharper peaks, while advanced models (IRSN, Morino) spread the plume more → lower peak TEDE. It was shown that TEDE peaks are relatively close to the source (≈0.3–0.6 km) and that there is significant inter-model heterogeneity around the source. Figures 20 and 21 show stability classes B and C that are rather unstable.Dose peaks become more noticeable at mid-distances (0.5–5 km) with higher TEDE values than Class A. less turbulence than in Class A The plume remains nearer the ground and is narrower. Otherwise, there is significant instability, a maximum TEDE of 0.4–0.7 km, and a slower decay than in A and B. Figure 22: A neutral environment Consistency Class D: Demonstrate that balanced turbulence and advection, a plume that spreads steadily but slowly because TEDE declines more smoothly with distance, and models that converge more closely than in unstable situations. Stable atmospheric stability classes E and F are shown in Figures 23 and 24.-Prove that strong vertical confinement, weak turbulence, and The plume stays concentrated close to the ground, and the physical contours are visible. Higher far-field TEDE in comparison to unstable situations, lower near-source TEDE Longer plume travel with less dilution, TEDE over large distances (20–80 km), and a rapid increase in arrival time . Figure 25 for the RASCAL investigation :TEDE(A) > TEDE(B) > TEDE(C) > TEDE(D) > TEDE(E) > TEDE(F) (near source) Because unstable air keeps the plume close to receptors early, Stable air moves the dose downwind and delays the plume.

For IRSN and EAEA comparisons, Figures 29–30 display wind that varies over time, vertical diffusion, and deposition physics .They exhibit realistic arrival times, strong sensitivity to stability class, and smooth dosage decay.

International Journal of Environmental Sciences
ISSN 2519-5549 (online)
Vol.9, Issue 1, No.1. pp 1 - 28, 2026
www.iprjb.org

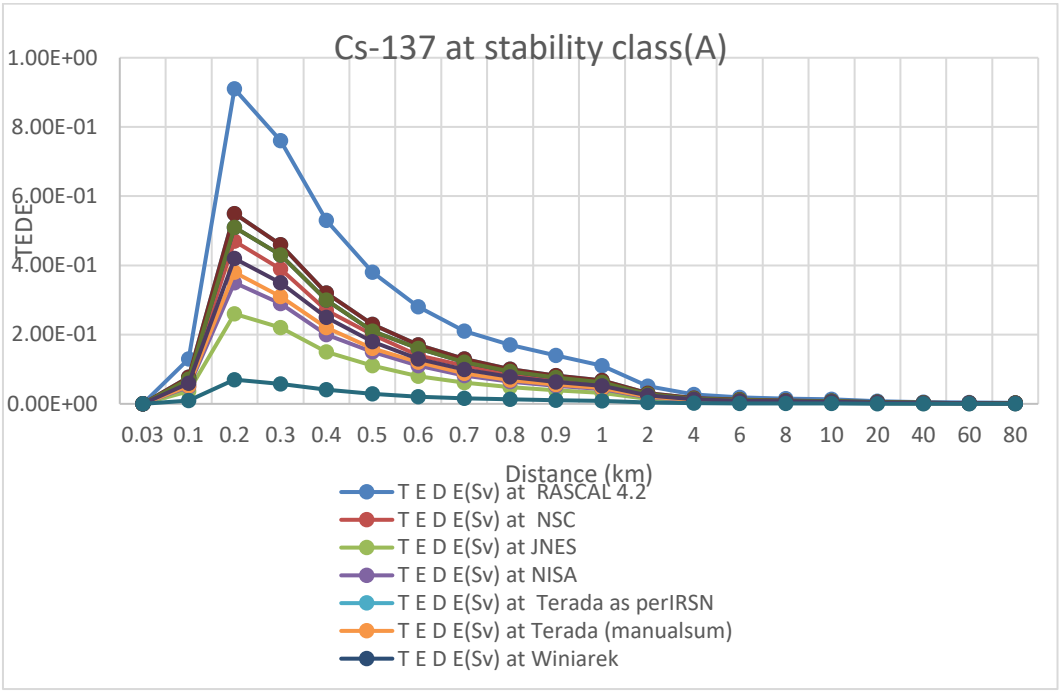

Figure 19: TEDE at stability class(A) for different studies

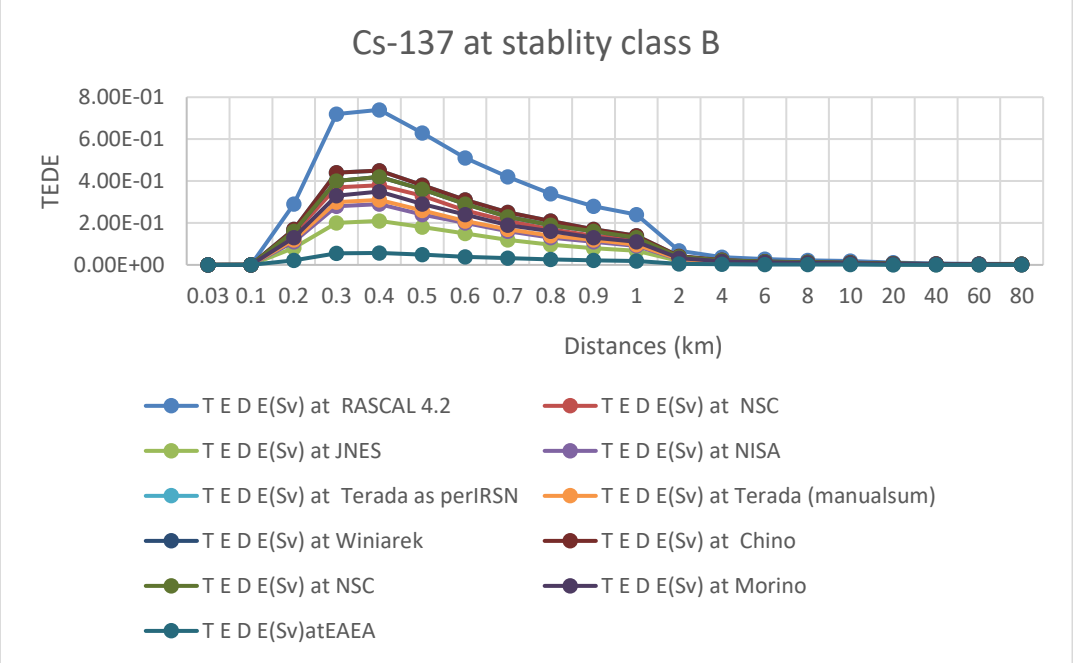

Figure 20: TEDE at stability class(B) for different studies

International Journal of Environmental Sciences
ISSN 2519-5549 (online)
Vol.9, Issue 1, No.1. pp 1 - 28, 2026
www.iprjb.org

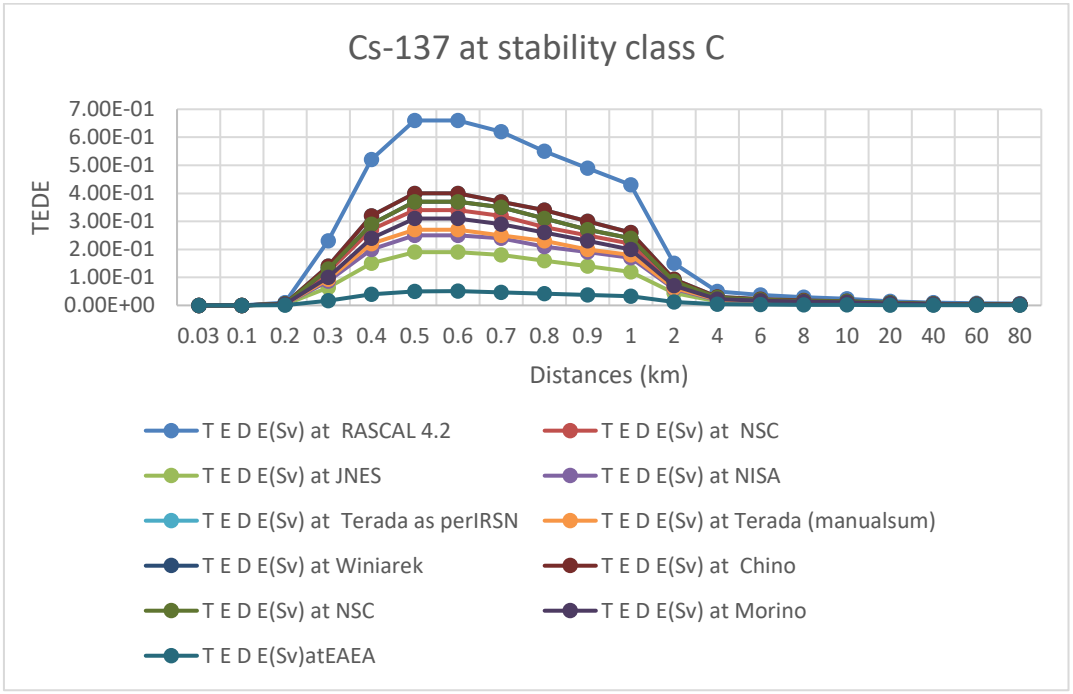

Figure 21: TEDE at stability class(C) for different studies

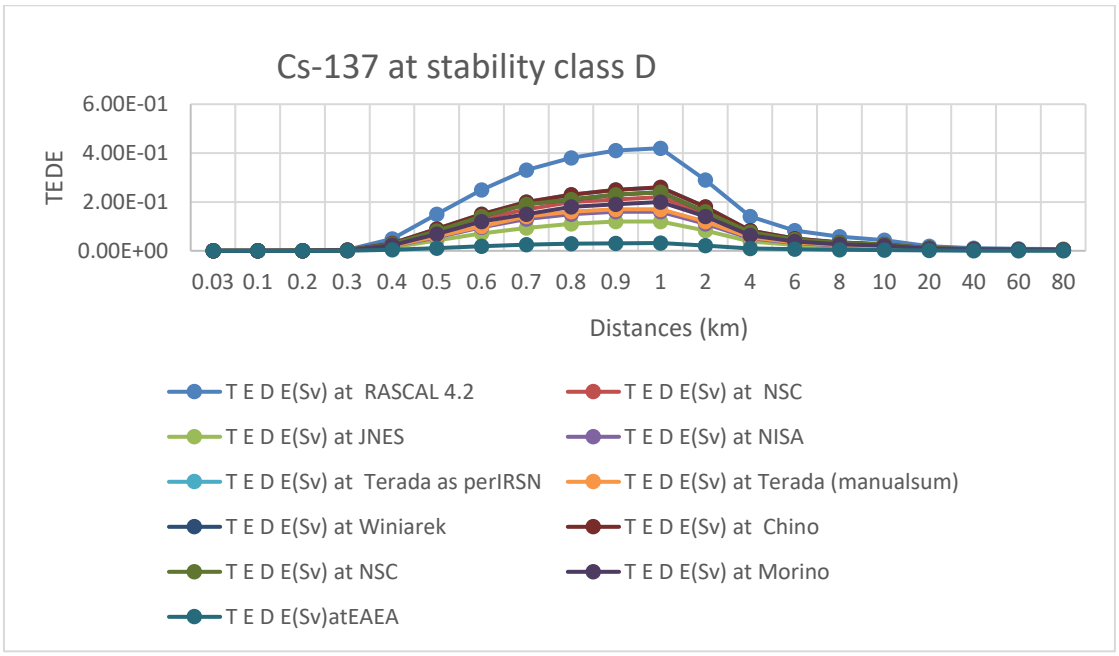

Figure 22: TEDE at stability class(D) for different studies

International Journal of Environmental Sciences
ISSN 2519-5549 (online)
Vol.9, Issue 1, No.1. pp 1 - 28, 2026
www.iprjb.org

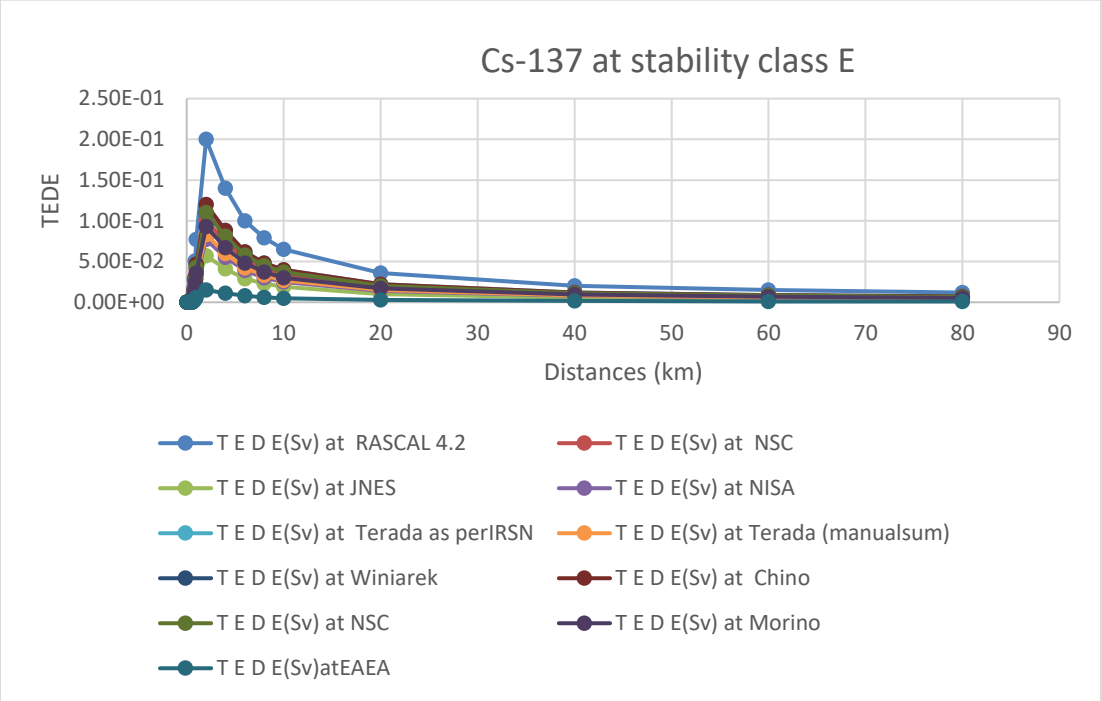

Figure 23: TEDE at stability class(E) for different studies

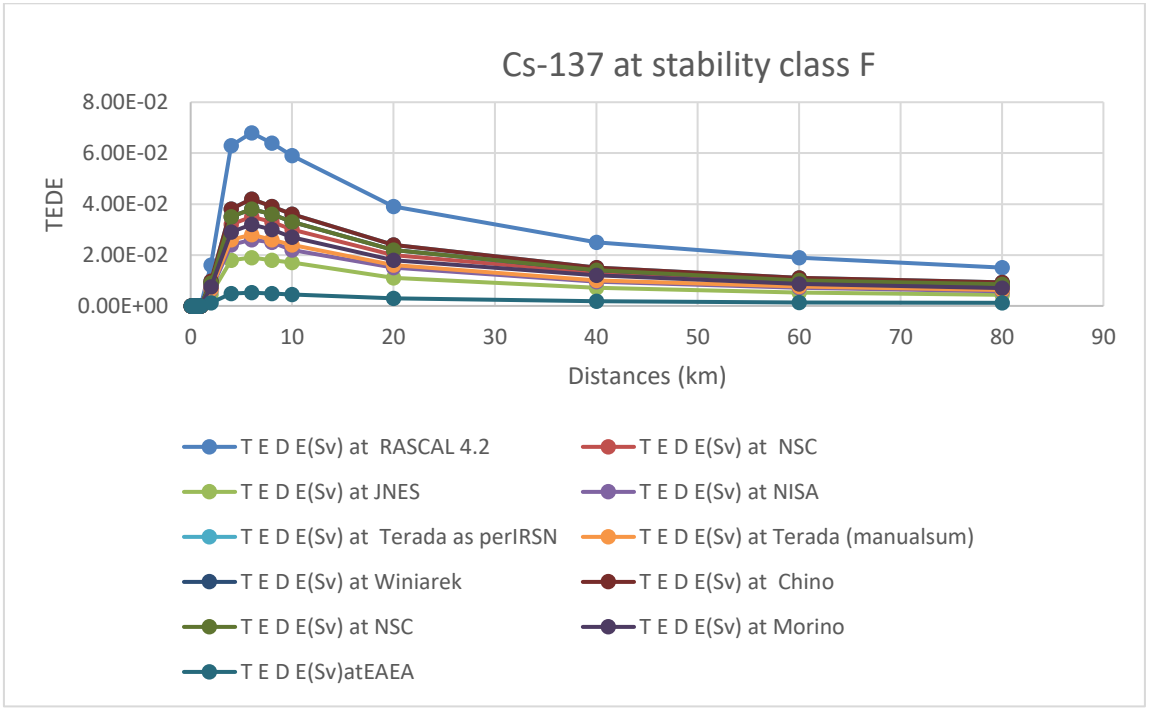

Figure 24: TEDE at stability class(F) for different studies

International Journal of Environmental Sciences
ISSN 2519-5549 (online)
Vol.9, Issue 1, No.1. pp 1 - 28, 2026
www.iprjb.org

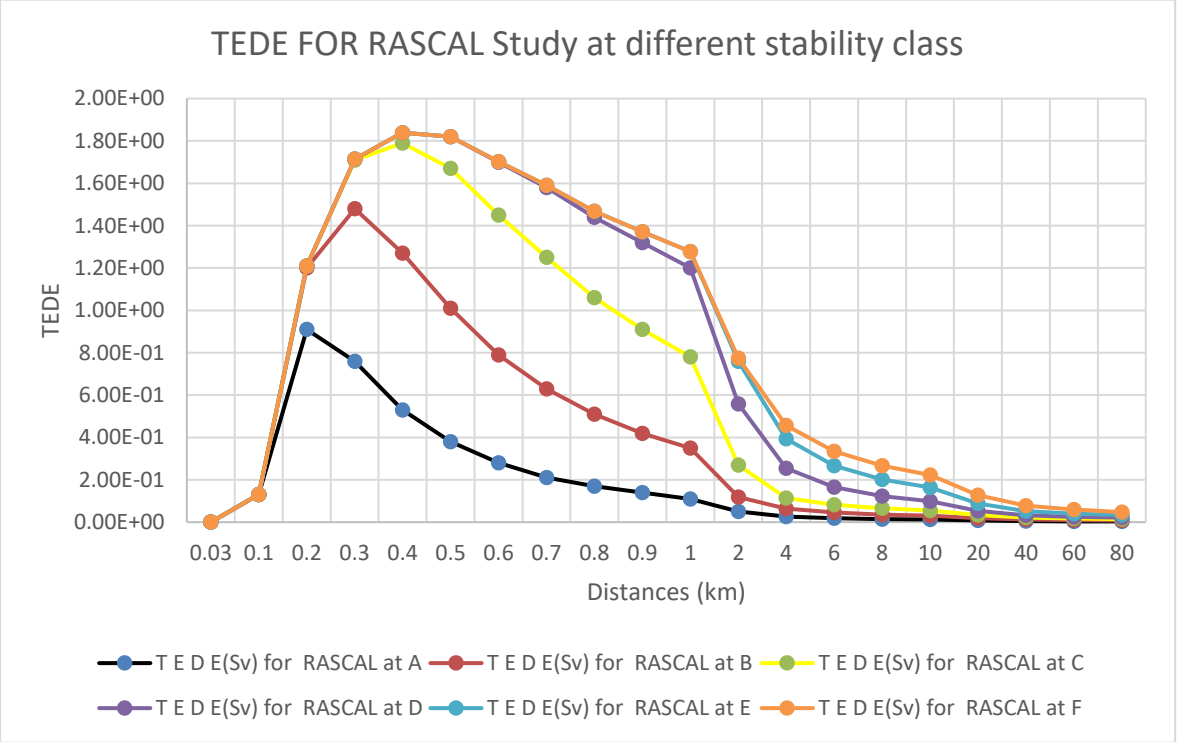

Figure 25: Comparison between TEDE of RASCAL at different stability class

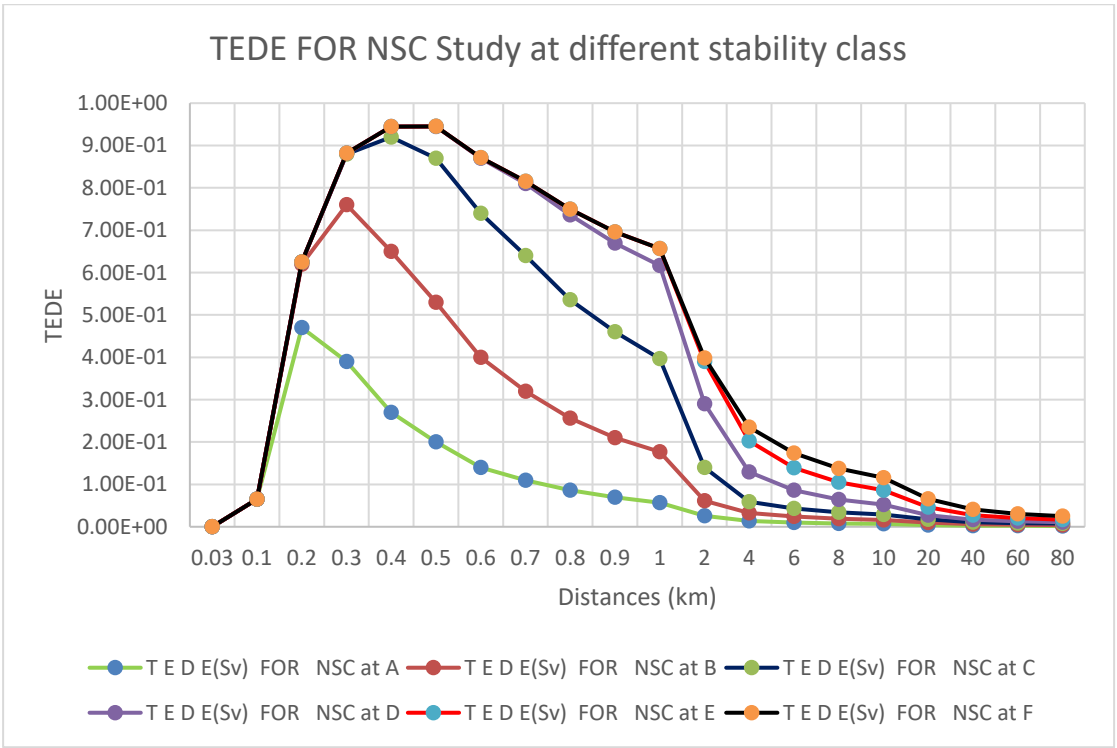

Figure 26: Comparison between TEDE of NSC at different stability class

International Journal of Environmental Sciences
ISSN 2519-5549 (online)
Vol.9, Issue 1, No.1. pp 1 - 28, 2026
www.iprjb.org

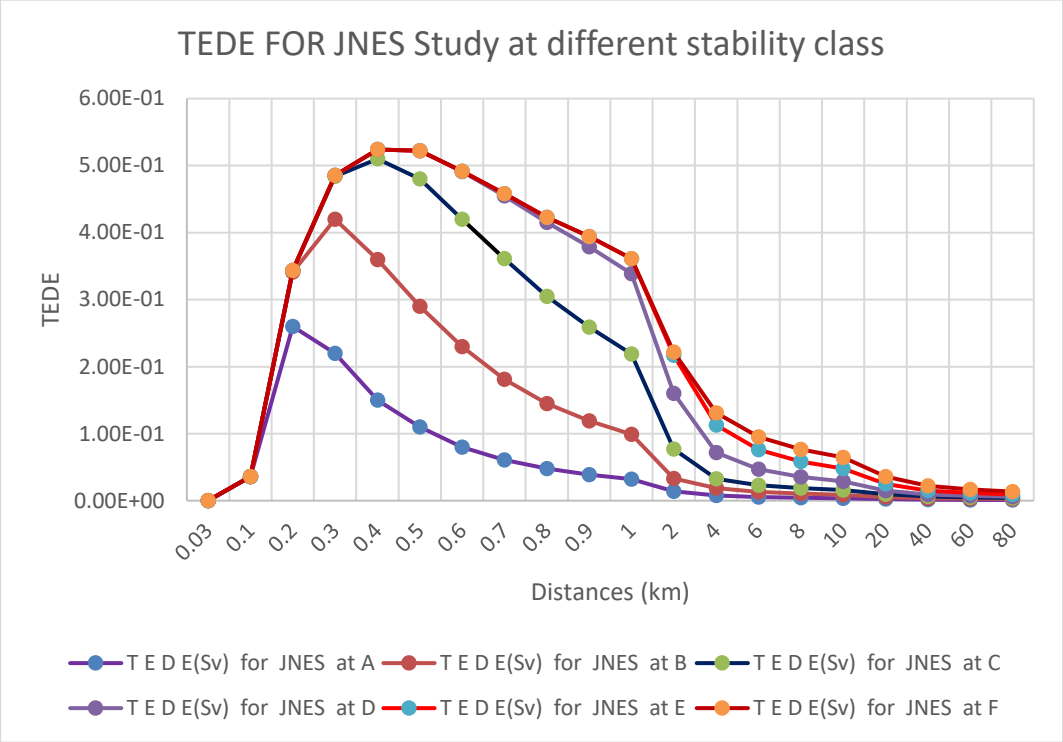

Figure 27: Comparison between TEDE of JNES at different stability class

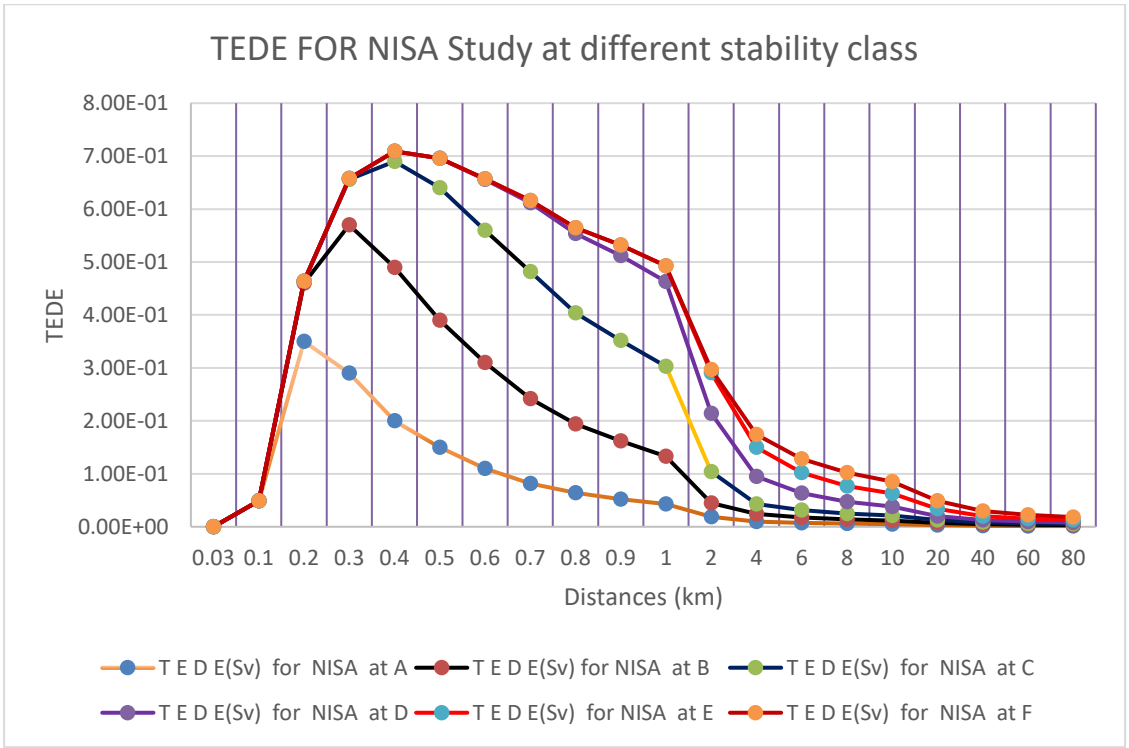

Figure 28: Comparison between TEDE of NISA at different stability class

International Journal of Environmental Sciences
ISSN 2519-5549 (online)
Vol.9, Issue 1, No.1. pp 1 - 28, 2026
www.iprjb.org

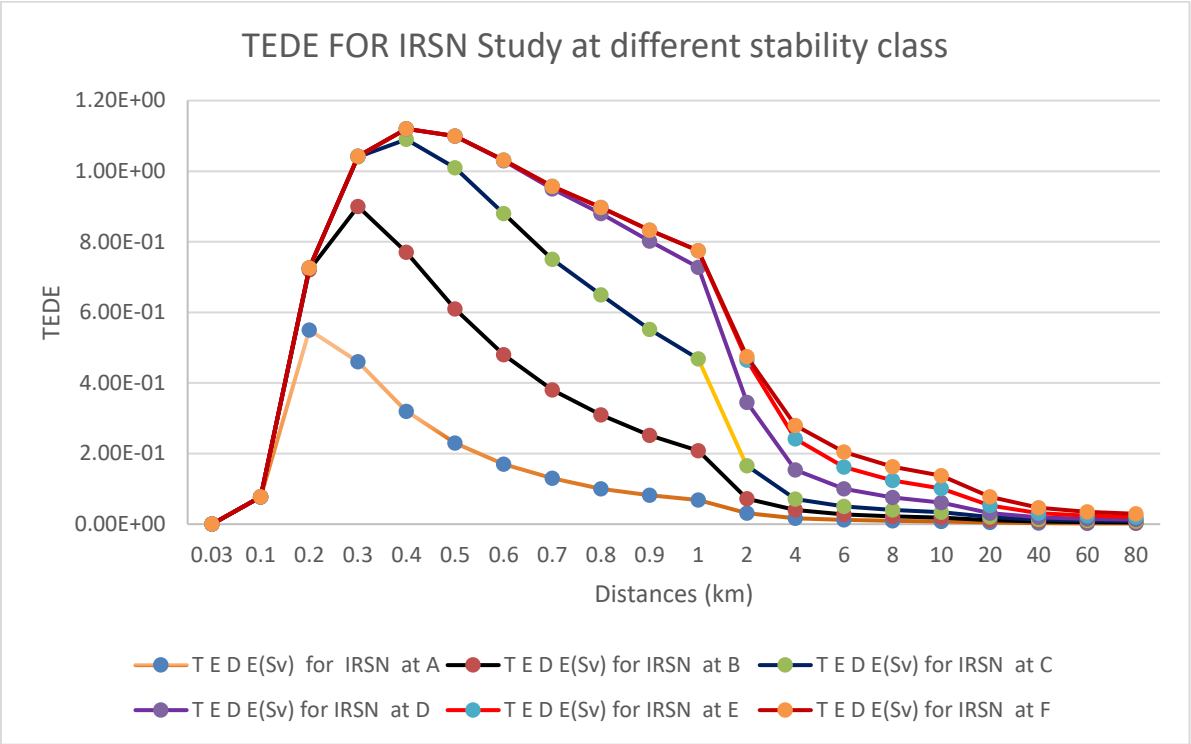

Figure 29: Comparison between TEDE of IRSN at different stability class

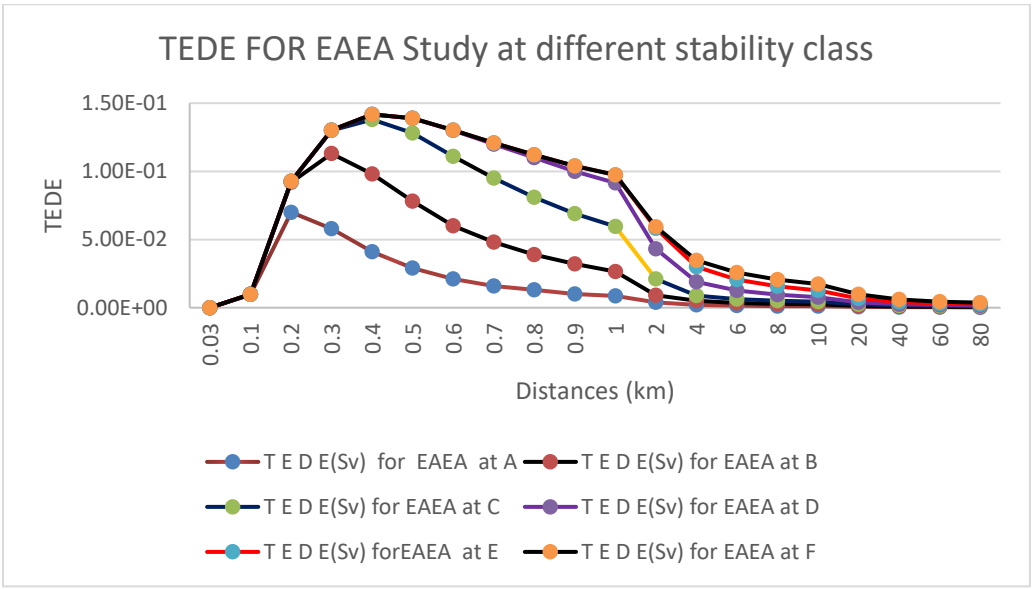

Figure 30: Comparison between TEDE of EAEA at different stability class

International Journal of Environmental Sciences
ISSN 2519-5549 (online)
Vol.9, Issue 1, No.1. pp 1 - 28, 2026
www.iprjb.org

Table (2(a,b)): TEDE comparison at stability class C, demonstrate Because of model type, RASCAL has the highest TEDE, EAEA has the lowest, and Terada and IRSN are in the middle. The maximum TEDE happens at 0.4–0.6 km, while RASCAL is conservative, IRSN is advanced turbulence, deposition, and EAEA is conservative distance smoothing.

Table (2 (a)): TEDE for different studies at stability class C

DISTANCE (Km)	T E D E(Sv) at RASCAL 4.2	T E D E(Sv) at NSC	T E D E(Sv) at JNES	T E D E(Sv) at NISA	T E D E(Sv) at Terada as perIRSN	T E D E(Sv) at Terada (manualsum)
0.1	3.70E-11	1.90E-11	1.00E-11	1.40E-11	2.20E-11	1.50E-11
0.2	9.50E-03	4.90E-03	2.70E-03	3.70E-03	5.80E-03	3.90E-03
0.3	2.30E-01	1.20E-01	6.40E-02	8.60E-02	1.40E-01	9.30E-02
0.4	5.20E-01	2.70E-01	1.50E-01	2.00E-01	3.20E-01	2.20E-01
0.5	6.60E-01	3.40E-01	1.90E-01	2.50E-01	4.00E-01	2.70E-01
0.6	6.60E-01	3.40E-01	1.90E-01	2.50E-01	4.00E-01	2.70E-01
0.7	6.20E-01	3.20E-01	1.80E-01	2.40E-01	3.70E-01	2.50E-01
0.8	5.50E-01	2.80E-01	1.60E-01	2.10E-01	3.40E-01	2.30E-01
0.9	4.90E-01	2.50E-01	1.40E-01	1.90E-01	3.00E-01	2.00E-01
1	4.30E-01	2.20E-01	1.20E-01	1.70E-01	2.60E-01	1.80E-01
2	1.50E-01	7.90E-02	4.40E-02	5.90E-02	9.30E-02	6.30E-02
4	5.00E-02	2.60E-02	1.40E-02	1.90E-02	3.10E-02	2.10E-02
6	3.70E-02	1.90E-02	1.00E-02	1.40E-02	2.20E-02	1.50E-02
8	2.90E-02	1.50E-02	8.20E-03	1.10E-02	1.80E-02	1.20E-02
10	2.40E-02	1.30E-02	6.90E-03	9.30E-03	1.50E-02	1.00E-02
20	1.50E-02	7.60E-03	4.20E-03	5.60E-03	8.90E-03	6.10E-03
40	9.40E-03	4.80E-03	2.70E-03	3.60E-03	5.70E-03	3.90E-03
60	7.30E-03	3.80E-03	2.10E-03	2.80E-03	4.40E-03	3.00E-03
80	6.20E-03	3.20E-03	1.80E-03	2.40E-03	3.70E-03	2.50E-03

International Journal of Environmental Sciences
ISSN 2519-5549 (online)
Vol.9, Issue 1, No.1. pp 1 - 28, 2026
www.iprjb.org

Table (2 (b)) :- TEDE for different studies at stability class C

DISTANCE (km)	T E D E(Sv) at Winiarek	T E D E(Sv) at Chino	T E D E(Sv) at NSC	T E D E(Sv) at Morino	T E D E(Sv)atEAEA
0.1	2.10E-11	2.20E-11	2.10E-11	1.70E-11	2.80E-12
0.2	5.30E-03	5.80E-03	5.30E-03	4.40E-03	7.30E-04
0.3	1.30E-01	1.40E-01	1.30E-01	1.00E-01	1.70E-02
0.4	2.90E-01	3.20E-01	2.90E-01	2.40E-01	4.00E-02
0.5	3.70E-01	4.00E-01	3.70E-01	3.10E-01	5.00E-02
0.6	3.70E-01	4.00E-01	3.70E-01	3.10E-01	5.10E-02
0.7	3.50E-01	3.70E-01	3.50E-01	2.90E-01	4.70E-02
0.8	3.10E-01	3.40E-01	3.10E-01	2.60E-01	4.20E-02
0.9	2.70E-01	3.00E-01	2.70E-01	2.30E-01	3.70E-02
1	2.40E-01	2.60E-01	2.40E-01	2.00E-01	3.30E-02
2	8.60E-02	9.30E-02	8.60E-02	7.10E-02	1.20E-02
4	2.80E-02	3.10E-02	2.80E-02	2.30E-02	3.90E-03
6	2.00E-02	2.20E-02	2.00E-02	1.70E-02	2.80E-03
8	1.60E-02	1.80E-02	1.60E-02	1.30E-02	2.20E-03
10	1.40E-02	1.50E-02	1.40E-02	1.10E-02	1.90E-03
20	8.30E-03	8.90E-03	8.30E-03	6.80E-03	1.10E-03
40	5.20E-03	5.70E-03	5.20E-03	4.30E-03	7.20E-04
60	4.10E-03	4.40E-03	4.10E-03	3.40E-03	5.60E-04
80	3.50E-03	3.70E-03	3.50E-03	2.90E-03	4.70E-04

Table (3): demonstrate that stable class F has the longest arrival time, unstable class C has the fastest plume arrival, and TEDE rises with earlier and denser plume arrivals because emergency reaction time is highly dependent on stability. Faster Arrival in Unstable Conditions: Because of improved vertical mixing and more efficient transmission, the Class C plume arrives earlier than the F.

International Journal of Environmental Sciences
ISSN 2519-5549 (online)
Vol.9, Issue 1, No.1. pp 1 - 28, 2026
www.iprjb.org

Table (3) : Comparison between TEDE a function of downwind distance and Arrival time of the plume for IRSN study at different stability class

DISTANCE (km)	T E D EA(sv) at stability class C	T E D EA(sv) at stability class D	T E D EA(sv) at stability class F	ARRIVAL TIME (hour:min) at stability class C	ARRIVAL TIME (hour:min) at stability class D	ARRIVAL TIME (hour:min) at stability class F
0.1	2.20E-11	0.00E+00	0.00E+00	<00:01	<00:01	<00:01
0.2	5.80E-03	1.70E-06	0.00E+00	<00:01	<00:01	<00:01
0.3	1.40E-01	2.50E-03	0.00E+00	0:01	00:01	<00:01
0.4	3.20E-01	3.00E-02	0.00E+00	0:01	00:01	<00:01
0.5	4.00E-01	8.90E-02	1.80E-15	0:02	00:02	00:01
0.6	4.00E-01	1.50E-01	1.90E-11	0:02	00:02	00:01
0.7	3.70E-01	2.00E-01	5.60E-09	0:03	00:02	00:01
0.8	3.40E-01	2.30E-01	2.40E-07	0:03	00:03	00:01
0.9	3.00E-01	2.50E-01	3.20E-06	0:04	00:03	00:01
1	2.60E-01	2.60E-01	2.10E-05	0:04	00:04	00:02
2	9.30E-02	1.80E-01	9.80E-03	0:09	00:08	00:04
4	3.10E-02	8.30E-02	3.80E-02	0:18	00:16	00:08
6	2.20E-02	5.00E-02	4.20E-02	0:27	00:25	00:12
8	1.80E-02	3.50E-02	3.90E-02	0:37	00:33	00:16
10	1.50E-02	2.70E-02	3.60E-02	0:46	00:42	00:20
20	8.90E-03	1.10E-02	2.40E-02	1:32	01:24	00:41
40	5.70E-03	6.60E-03	1.50E-02	3:05	02:49	01:22
60	4.40E-03	5.00E-03	1.10E-02	4:38	04:14	02:04
80	3.70E-03	4.20E-03	9.20E-03	6:11	05:39	02:45

Conclusion

This work presents a comprehensive comparison of several studies such as (RASCAL, NSC, JNES, NISA, IRSN–Terada, Winiarek , Morino, and EAEA) , that have calculated source term of Fukushima accident ,which used as input data in HOTSOT code for estimating the total equivalent radiation dose (TEDE) from Cs-137 deposition resulting from an atmospheric nuclear emission. Because of conservative assumptions and a simplified Gaussian diffusion, models like RASCAL and NSC show strong dosage peaks near the source with narrow columns. Because they more accurately depict atmospheric turbulence, vertical mixing, and moist deposition, models like IRSN, Terada, Morino, and EAEA exhibit a wider diffusion and lower peak doses. Rainfall has a significant impact on ground-level deposition (wet deposition), resulting in erratic "hot spots," whereas substantial vertical mixing reduces unpredictability. Stable weather (E–F) has narrow columns, lower doses near the source but higher at long distances with a longer arrival time, where the cloud's arrival time increases with increasing atmospheric stability. Unstable weather (A–C) has wide spread, rapid dilution of focus, TEDE peaks close to the source, and neutral weather (D) has average behavior and greater convergence between models.

REFERENCES

[1] Estimation of the time-dependent radioactive source-term from the Fukushima nuclear power plant accident using atmospheric transport modelling .2012 J.Environ.Radioact

[2] INPO Special Report - Special Report on the Nuclear Accident at the Fukushima Daiichi Nuclear Power Station, INPO 11-005, Revision 0, November 2011.

[3] SANDIA Report, Fukushima Daiichi Accident Study (Status as of April 2012), SAND2012-6173, July 2012.

[4] SANDIA Report, Fukushima Daiichi Accident Study (Status as of April 2012), SAND2012-6173, July 2012.

[5] INPO Special Report - Special Report on the Nuclear Accident at the Fukushima Daiichi Nuclear Power Station, INPO 11-005, Revision 0, November 2011.

[6] EPRI Report, Fukushima Technical Evaluation Phase 1—MAAP5 Analysis, 1025750, April 2013.

[7] Technical Knowledge of the Accident at Fukushima Dai-ichi Nuclear Power Station; http://www.nsr.go.jp/archive/nisa/english/press/2012/06/en20120615-1-1.pdf http://www.nsr.go.jp/archive/nisa/english/press/2012/06/en20120615-1-2.pdf, NISA, March - June 2012, in particular Chapter V: Containment System.

[8] NUREG-1940. RASCAL 4: Description of Models and Methods, December 2012.

[9] TEPCO Press Release 24 May 2012, Estimation of Radioactive Material Released to the Atmosphere during the Fukushima Daiichi NPS Accident, http://www.tepco.co.jp/en/press/corp- com/release/betu12_e/images/120524e0205.pdf

[10] H. Terada, G. Katata, M. Chino, H. Nagai, Atmospheric discharge and dispersion of radionuclides during the Fukushima Dai-ichi Nuclear Power Plant accident. Part II: verification of the source term and analysis of regional-scale atmospheric dispersion, Journal of Environmental Radioactivity, Volume 112, 141-154, October 2012.

[11] H. Terada, G. Katata, M. Chino, H. Nagai, Atmospheric discharge and dispersion of radionuclides during the Fukushima Dai-ichi Nuclear Power Plant accident. Part II: verification of the source term and analysis of regional-scale atmospheric dispersion, Journal of Environmental Radioactivity, Volume 112, 141-154, October 2012. , but total amounts calculated by spreadsheet.

[12] V. Winiarek, M. Bocquet, O. Saunier, A. Mathieu, Estimation of errors in the inverse modeling of accidental release of atmospheric pollutant: Application to the reconstruction of the cesium-137 and iodine-131 source terms from the Fukushima Daiichi power plant, J. Geophys. Res. Atmospheres, Volume 117, Issue D5, 16 March 2012.

[13] M. Chino; H. Nakayama, H. Nagai, H. Terada, G. Katata, H. Yamazawa, Preliminary Estimation of Release Amounts of 131I and 137Cs accidentally discharged from the Fukushima Daiichi Nuclear Power Plant into the Atmosphere, Journal of Nuclear Science and Technology, Vol. 48, No. 7, p. 1129–1134, 2011.

[14] Press Release 12 April 2011; data taken from [9].

[15] Y. Morino, T. Ohara, M. Nishizawa, Atmospheric behavior, deposition, and budget of radioactive materials from the Fukushima Daiichi nuclear power plant in March 2011, Geophysical Res. Letters 38, 7, 2011.

[16] M.K. Shaat, Amr Abdelhady, Rowayda F. Mahmoud" Radiological Impact due to Atmospheric Releases of the Source Term for F-D, Unit 1, Using HOTSPOT Code" Annals of Ecology and Environmental Science Volume 3, Issue 1, 2019, PP 33-39 - ISSN 2637-5338

[17] mariachiara carestia, andrea malizia, oscar barlascini, eugenio fiorini, paolo maurizio soave, gianna latini, orlando cenciarelli, fabrizio d'amico, carlo bellecci, pasquale gaudio" use of the "hotspot" code for safety and security analysis in nuclear power plants: a case stud. environmental engineering and management journal april 2016, vol.15, no. 4, 905-912.

[18] Environmental Protection Agency (EPA). Limiting Values Radionuclide Intake and Air Concentration, and Dose Conversion Factors for Inhalation, Submersion, and Ingestion. EPA, Federal Guidance Report 11, Washington DC, 1988.

[19] Rentai, Y. Atmospheric dispersion of radioactive material in radiological risk assessment and emergency response. Progress in Nuclear Science and Technology, Vol. 1, 2011, pp. 7-13.

[20] Gallo, R., De Angelis, P., Malizia, A., Conetta, F., Di Giovanni, D., et al. Development of a georeferencing software for radiological diffusion in order to improve the safety and security of first responders. Defence S&T Technical Bullettin Vol. 6, 2013, pp. 21-32

[21] M.K. Shaat, Amr Abdelhady, Rowayda F. Mahmoud"Radiological Impact due to Atmospheric Releases of the Source Term for F-D, Unit 1, Using HOTSPOT Code" Annals of Ecology and Environmental Science Volume 3, Issue 1, 2019, PP 33-39

[22] Leone, J.M., Nasstrom, J.S., Maddix, D.M., Larson, D.J., Sugiyama, G.S., and Ermak, D.L. *Lagrangian Operational Dispersion Integrator (LODI) Users Guide*, UCRL-AM-212798, Lawrence Livermore National Laboratory, 2001

[23] Likhtarev I. A. et al., ―Chernobyl Accident: Retrospective and Prospective Estimates of External Dose of the Population of Ukraine,‖ Health Physics, March 2002, Volume 82, No. 3, pp. 290 -303,

[24] Federal Radiological Monitoring and Assessment Center (FRMAC), "FRMAC Assessment Manual – Tables, Charts, Worksheet, Glossary, References," Volume 2, p. 124. SAND2003-1072P, April, 2003.

[25] Eckerman, K. F., Leggett, R. W. Personal communication, DCFPAK 2.2: Updated Dose and Risk Coefficient Database for Rapid Assessment of Radiation Doses, 2010.